Appl. Phys. A 63, 461–465 (1996)

Applied Physics A Materials Science & Processing

Laser-surface-alloying of the iron based superalloy Incoloy-800H with Al

A. Gutiérrez, J. de Damborenea

Departamento de Corrosión y Protección, CENIM (CSIC) Avda. Gregorio del Amo 8, E-28040 Madrid, Spain

Received: 14 February 1996 / Accepted: 1 July 1996

Abstract. Laser surface alloying by the powder feed method of the iron based superalloy Incoloy 800H with aluminium has been carried out. The effects of different preparation parameters, like laser scan speed and powder feed rate, on the morphology of the alloyed zone have been investigated. Microstructure and composition have been determined by scanning electron microscopy (SEM), optical microscopy, and x-ray fluorescence spectroscopy. Three different phases with different Al-content have been distinguished. The observed Al-enrichment at the surface, the presence of Ni-Al and Fe-Al intermetallic compounds, and the considerable grain refining of the alloyed zone with respect to the substrate, make this surface modification technique a very good method to improve the corrosion behaviour of the Incoloy 800H superalloy.

PACS: 81.65, 42.70.H, 81.05.Bx

In the last decades there has been a continuous development of heat resistant new materials with good mechanical properties, such as strength and wear resistance, aimed to attend to the needs of the gas turbine industry [1, 2]. Surface properties of such materials are crucial, since most processes influencing their lifetime, like wear or corrosion, occur at the surface [3]. Surface modified materials constitute a very good option, since they have their surface properties improved while conserving the good mechanical behaviour of the bulk material [4, 5]. From the corrosion point of view, any temperature increase involves a higher oxidation rate. Protective coatings, based on Cr_2O_3 and Al_2O_3 scales, can slow down the corrosion process to a very high extent [4, 6].

Laser surface modification of materials constitutes a very good method to improve their surface properties due, among other things, to the high power densities involved [7, 8, 9]. Laser surface hardening can give rise to new phases due to the very high heating and cooling rates, which lead to conditions very far from equilibrium and also produce considerable grain refining [10]. In laser surface cladding, a protective coating is obtained by melting powder material of different compositions on the surface to be treated, with minimum dilution of the melt into the bulk material [7, 9, 11, 12, 13]. In the process of laser surface alloying there is a simultaneous melting of substrate and powder materials, allowing the formation of a protective alloyed coating [14, 15, 16, 17]. Due to the very good protective characteristics of Al_2O_3 scales, which can reduce oxidation rates at high temperatures up to a factor 8 [18], Al is a commonly used material in laser surface alloying [13, 14, 15].

The iron based superalloy Incoloy 800H combines good strength and resistance to oxidation and carburation in high temperatures and many aqueous environments. This good corrosion behaviour may be improved by incorporating Al at the surface. Al_2O_3 scales would lead to a higher resistance to oxidation at high temperatures, while the Cr content of the base alloy would maintain its resistance to carburation and sulfidation [18]. In the present work, a study of the composition and morphology of laser surface alloyed Incoloy 800H with aluminium is reported. The high Cr content of the base alloy, together with the highly protective properties of the Al-rich coating, make this surface modified material very interesting in high-temperature anti-corrosive applications. Its high-temperature oxidation behaviour will be the subject of a future work.

1 Experimental details

The method used for laser surface alloying was powder injection, by which the alloying material, in powder form, is directed onto the surface of the material to be alloyed at the point where the laser is being focused, leading to the simultaneous melting of both materials [16]. Pure aluminium powder (99.9%) was fed into the melting pool by means of a stream of argon. A powder feed unit equipped with a flow balance was used to control the Al powder feed rate [8, 11, 12]. The Fe based superalloy Incoloy 800H, with nominal composition (wt%) Fe 45.36, Ni 30.78, Cr 20.0, Co 0.87, Mn 0.71, Si 0.52, Cu 0.49, and Ti 0.33, was used as substrate material. Several samples, 5 mm thick, were cut from a rod of 60 mm diameter.

The laser employed was a CO_2 continuous wave laser (Spectra Physics) operated in multimode beam, with an out-

Correspondence to: A. Gutiérrez, E-mail: alejandro@pinar1.csic.es

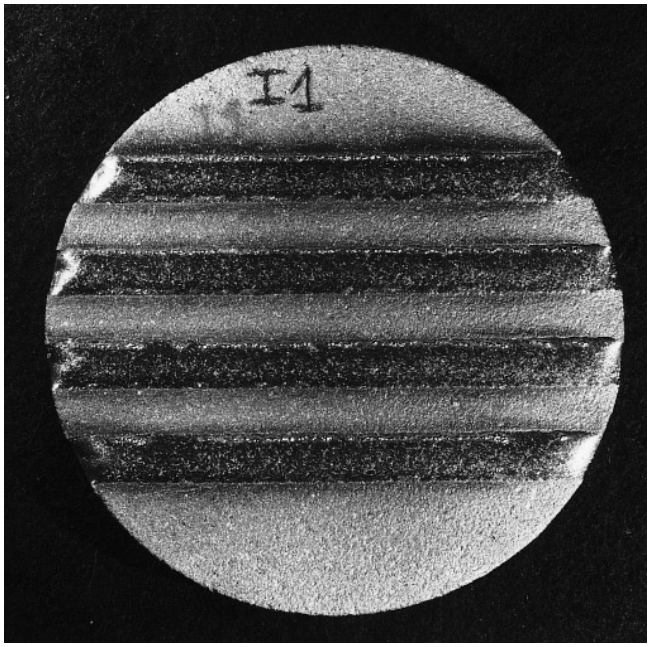

Fig. 1. Top view of a representative sample after laser treatment. The tracks were obtained by scanning the laser beam four times through the substrate surface at a scan speed of 800 mm/min while Al powder was being injected at a powder feed rate of 3 g/min. Note the low rugosity of the tracks with respect to the substrate

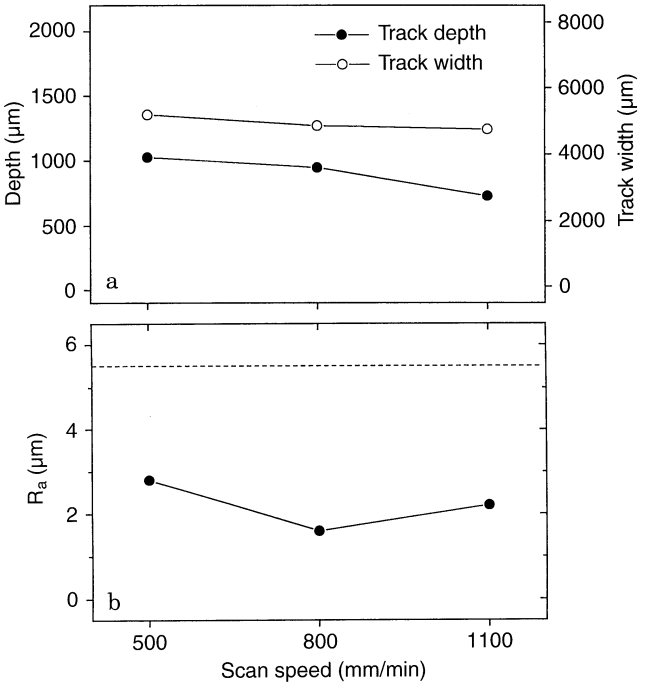

Fig. 2a,b. Evolution of the track depth and width **(a)**, as well as the rugosity **(b)** with respect to the laser scan speed

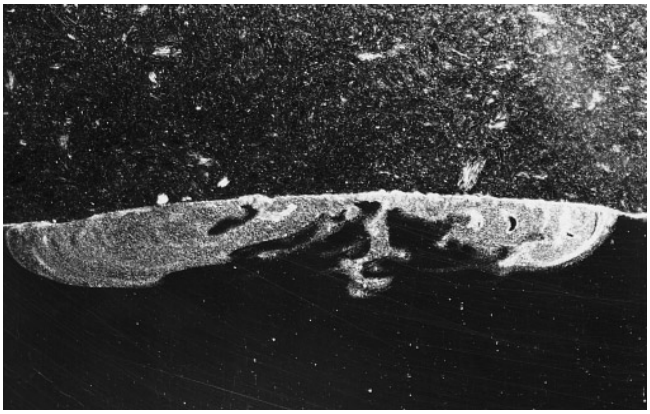

Fig. 3. Cross section of a track corresponding to the sample prepared with a 800 mm/min laser scan speed and 3 g/min powder feed rate. The image magnification is ×16. The sample was previously treated in order to optimize contrast between the different phases

put power of 5000 kW. The laser beam was focused onto the substrate surface, giving a spot area of 64 mm^2. In order to reduce losses caused by reflectivity from the substrate, samples were sand blasted prior to laser treatment. The laser beam was scanned onto the samples by moving them at a constant traverse speed. Several samples were obtained, using a powder feed rate of 3 g/min and different scan speeds (500 mm/min, 800 mm/min, 1100 min, and 1400 mm/min), in order to find the best alloying conditions.

The modified surfaces were studied by optical microscopy, scanning electron microscopy (SEM), and x-ray microprobe analysis (XMA). Metallographic observations were done on cross sections of the material, which were previously polished and chemically attacked in order to emphasize the different metallographic phases. SEM pictures and XMA spectra were obtained in a commercial JEOL-JXA 840 system with 15 keV incident electron energy. A Mitutoyo 401 Surftest was used to determine the roughness of the samples after laser treatment. Roughness measurements were related to the bare samples after sand blasting.

2 Results and discussion

Four tracks, prepared under the same conditions, were made on each sample, as shown in Fig. 1. All single tracks presented good aspect, homogeneity, and a relative low rugosity, with no cracks observed at first sight. No significant differences were observed between tracks made on the same sample, i.e., under the same conditions, showing the good statistical behaviour of the method and the good reproducibility of the modified surfaces.

Figure 2 shows the relationship between some morphological aspects of the laser alloyed zone and the scan traverse speed. In Fig. 2a the depth (left axis) and width (right axis) of the alloyed zone, as determined by metallographic observations on cross sections of the samples, are presented. Both magnitudes show a decreasing behaviour, since the supplied laser energy per unit surface area is also a decreasing function of the laser scan speed. Whereas the track width presents very small variations, the depth seems to be more sensitive to changes in the traverse speed. Both magnitudes show a low dependence on the traverse speed as compared with other systems [15], which can be due to differences in the intensity distribution of the laser beam, especially at the edge of the beam spot. These differences may be originated by the use of a different mode structure or a different beam size (3 mm in Ref. 15 vs. 8 mm in our case). Also the intrinsic properties of the treated material, especially the thermal conductivity, should play an important role. Figure 2b

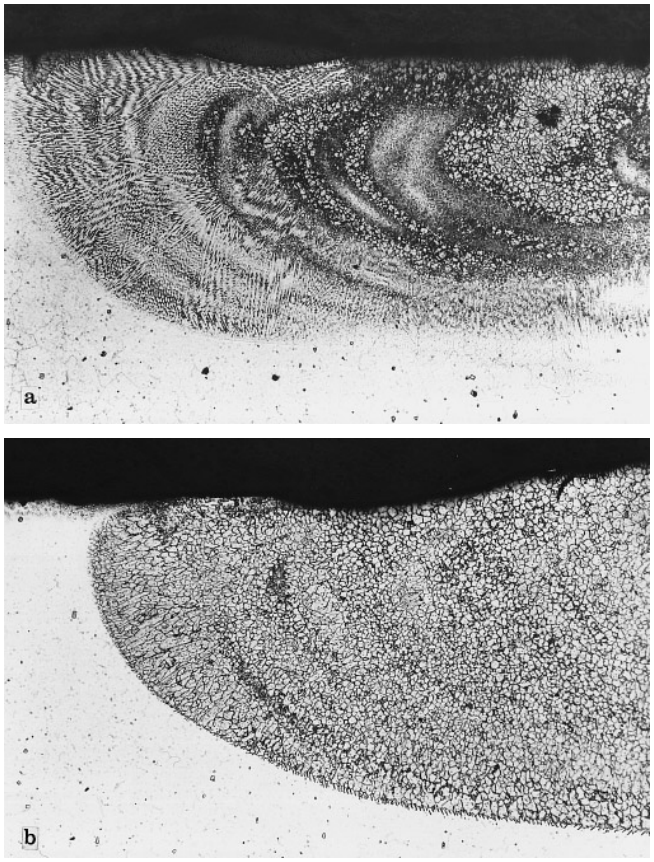

Fig. 4a,b. Detail of the region close to the track boundary of two samples, prepared at 1400 mm/min laser scan speed **(a)**, and 800 mm/min **(b)**, respectively. The image magnification is $\times 40$. The samples were previously treated in order to optimize the contrast between the different phases

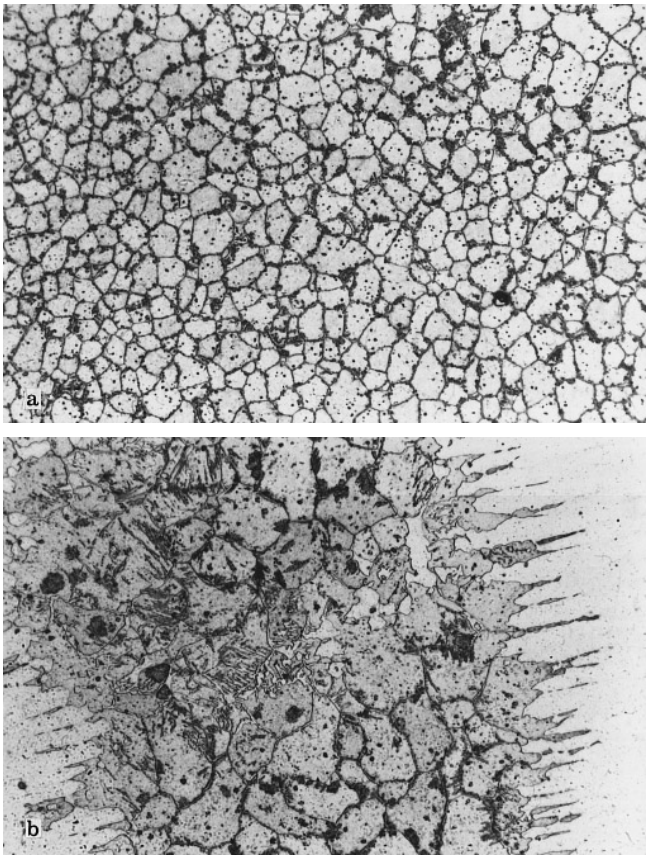

Fig. 5. Micrography of two different regions of a sample prepared at 800 mm/min laser scan speed and 3 g/min powder feed rate. **a** corresponds to the region close to the track boundary and **b** to the central part of the track. The magnification is $\times 200$

shows the roughness vs. traverse speed for the same samples. The dashed line corresponds to the roughness of the Incoloy-800H surface after sand blasting, measured in the longitudinal direction of the track. The much lower values (1.5-3 μm) obtained for the alloyed surfaces indicate the good surface finishing of the treatment, similarly to other systems previously studied [9].

In Fig. 3, a representative macrography of a track cross section is shown. It corresponds to a sample prepared with 800 mm/min traverse speed and a 3 g/min powder feed rate. Approximately the same morphology was observed for the rest of conditions, with only slight differences in the depth and width of the alloyed layer. As it can be observed in the figure, the region close to the track border presents higher homogeneity than the central part, where a lower apport of alloyed material can also be observed. Similar behaviour has been previously reported for other laser-applied coatings [19, 20]. The high temperature gradients inside the melt pool during the laser-surface interaction produce convective flows and thermocapilarity. The main force acting on these flows originates from variations in surface tension with temperature [21, 22]. The surface tension is low at the center of the pool, where the temperature is maximum, and high at the pool boundary, where the temperature is lower. This causes the melt to flow from center to border at the surface and in the opposite direction at the interface, giving rise to the formation of whirls of material flow. Since flow velocities at the surface are much higher than inside, the whirls are confined to the borders of the melt pool. This explains the lower apport of alloyed material at the central part, as well as its lower homogeneity as compared to the regions close to the border. A possibility to make this central part more homogeneous would be to produce tracks with an overlap close to 50%.

Relative densities of substrate and alloying material may influence the pool morphology, especially if the alloying material is heavier than the substrate [20]. In our case the alloying material density is much lower than the substrate density, so we can assume that the surface tension gradient is the only force acting on the melt flow. This force leads to the formation of whirls which carry most of the material flow, as mentioned above. Assuming a flow velocity of $\approx$ 2 m/s [19] the whirls would complete one cycle in $\approx$ 2.5 ms, resulting in 6-7 cycles for a laser scan speed of 500 mm/min, and only 2 cycles for 1400 mm/min. Since homogeneity is directly related to the number of cycles, samples prepared at higher scan speeds are expected to be less homogeneous. This behaviour is illustrated in Fig. 4, where the region close to the border of two samples prepared at different scan speeds is shown. Figure 4a corresponds to the highest speed, 1400 mm/min, and Fig. 4b to 800 mm/min. In both cases a considerable grain refining with respect to the substrate is observed. However, whereas the sample grown at 800 mm/min shows uniform grain size and form distribu-

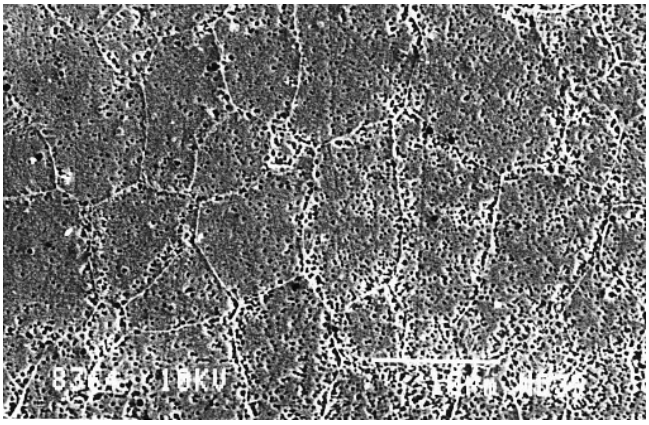

Fig. 6. SEM image of a region close to the track boundary corresponding to a sample prepared at 800 mm/min laser scan speed and 3 g/min powder feed rate

tions, the sample grown at 1400 mm/min has a less homogeneous appearance, and consists of several regions of different grain sizes and forms, with some poorly-mixed zones also visible. The pool/substrate interface looks also different, being more abrupt in the low scan-speed case, with no intermediate mixed zone, similarly to the case of laser surface cladding [7, 16]. A layered, onion-like superstructure can be observed in both cases, though in a more pronounced way in Fig. 4a, confirming the whirled trajectory of the melt flow before solidifying.

Samples grown with a scan speed of 800 mm/min and a feed powder rate of 3 g/min show the best behaviour as far as homogeneity and alloy mixing are concerned. Figure 5 shows microscopic images of two regions of a sample prepared under these conditions. Figure 5a corresponds to the pool boundary region and Fig. 5b to the central part. Three different phases can be distinguished in figure 5a: a solid solution consisted of equiaxed grains, a second phase precipitated along the grain boundaries, and a third one composed of globular precipitates inside the grains. Additionally, a fourth phase forming an acicular structure inside the grains can be observed in some zones of the central part of the track, as shown in Fig. 5b, in regions with certain lack of homogeneity. The image corresponds to a portion of melt material moving into the base alloy by means of the convective forces described above.

In order to characterize the different phases observed in the metallographic study, the samples were probed by SEM and XMA. Figure 6 shows a representative SEM image of the pool boundary region of a sample similar to that shown in Fig. 5. The grained structure and the precipitates observed in the metallographic image are perfectly clear. In order to quantify the composition of the different phases found, an x-ray fluorescence analysis was made. The obtained spectra were corrected to take into account self-absorption and auto-ionization effects between the different elements in the sample. The results of such analysis are shown in Table 1. Relative compositions are expressed in atomic percent, and correspond to mean values obtained by measuring each phase at several points on the sample, with an upper limit of the standard deviation of 5% of the corresponding value. Phases A, B, and C correspond to the

Table 1. Results of the x-ray fluorescence analysis performed on the different phases observed. Phase A corresponds to the grained structure, phase B to the precipitates inside the grains, and phase C to the precipitates at the grain boundaries. The zone where each measurement was done is also indicated. For each phase, the relative element composition is expressed as atomic percent. The standard deviation of each value is lower than a 5% of this value

	Fe	Ni	Cr	Al	Si	Ti
Base alloy	46	30	21	–	1	0.4
Phase A, interface	40-41	27	18-20	11-13	1-2	–
Phase A, surface	40	25	19	14	1	0.3
Phase B, interface	30	20	15	30	2	3
Phase B, center	25	15	14	39	2	3.6
Phase B, surface	26	14	13	46	1	0.4
Phase C, interface	35	22	19	22	2	0.8

three phases observed both by optical microscopy and SEM, i.e., grains, inner precipitates, and precipitates at the grain boundaries, respectively. For phases A and B variations with the position inside the pool were observed, so data are presented separately. The main difference between phases is the aluminium content, which is lower for phase A, increases for phase C, and is maximum for phase B. Differences in Al concentration also account for the variations observed in phase A and B with the position inside the pool. They indicate an Al-enrichment at the surface, though changes in phase A are much lower than in phase B. Due to the complexity of the system, an exact identification of the different phases would be rather complicated. Nevertheless, we have made an approach based on three ternary phase diagrams: Fe-Cr-Al, Ni-Cr-Al, and Fe-Ni-Al [23]. In Table 2 we show the results of this analysis. Each column corresponds to one of the phase diagrams, in which one of the main elements is absent. The arrows indicate transformations upon cooling, with the corresponding temperature. It is important to note that, due to the extreme conditions out of equilibrium of the laser alloying process, one has to take into account not only the stable phases at room temperature, but also all phases that appear at higher temperatures. These phases may also exist, since the extremely fast quenching rate of the process may not allow them to evolve as in the equilibrium phase diagram, and they would coexist as metastable phases together with the equilibrium phases. Some conclusions may be extracted from Table 2. Phase A seems to consist of a solid solution, composed of all main elements, with some Ni-Al intermetallic compounds, especially Ni_3Al. The presence of very small Ni_3Al precipitates inside a Ni-Al solid solution has already been observed in different Ni-Cr-Al alloys [24].Though from the Fe-Ni-Al diagram the presence of Fe-Al compounds in phase A could also be possible (γ phase), this possibility is excluded by the Fe-Cr-Al diagram. Nevertheless, Fe atoms can replace Ni in Ni_3Al, forming Ni-Fe-Al intermetallic compounds [8, 11].Both phase B and phase C have a higher Al content than phase A, reaching the solubility limit of Al, which starts to react with Fe and Cr. Phase C seems to be composed of (Cr), Fe-Al and Fe-Ni-Al phases, together with the Ni-Al phases already present in phase A (FeAl, Fe_2Al, NiAl, Ni_3Al, and ($Fe_xNi_{1-x}Al_y$)). NiAl is expected to evolve towards Ni_3Al if the quenching rates are sufficiently slow [24], but we expect a mixture of both phases due to the very high quenching rate involved in

Table 2. Results of an analysis based on the ternary equilibrium phase diagrams of the main components of the three phases studied. The arrows correspond to phase transformations and the numbers above them to the temperatures at which they have been reported. In the last rows the correspondence between phase names and formulae for each diagram is shown

	Fe-Cr-Al	Ni-Cr-Al	Fe-Ni-Al
Phase A	(Cr,αFe)	$\beta \xrightarrow{1150} \alpha+\beta+\gamma \xrightarrow{850} \gamma+\gamma'$	$\beta+\gamma$
Phase B, interface	(Cr,αFe)$\xrightarrow{900}$(Cr,αFe)+$\alpha_2+\zeta_2 \xrightarrow{750} \eta+\alpha_2+\zeta_2$	$\zeta \xrightarrow{1150} \beta+\zeta \xrightarrow{850} \alpha+\beta+\gamma'$	β
Phase B, middle	(Cr,αFe)$\xrightarrow{900}$(Cr,αFe)+$\alpha_2+\zeta_2 \xrightarrow{750}$ (Cr,αFe)+$\eta+\alpha_2$	$\beta \xrightarrow{1150} \beta+\zeta \xrightarrow{1025} \alpha+\delta+\zeta \xrightarrow{850} \alpha+\beta+\gamma'$	β
Phase B, surface	(Cr,αFe)$\xrightarrow{900}$(Cr,αFe)+$\alpha_2+\zeta_2 \xrightarrow{750} \eta+\alpha_2+\zeta_2$	$\zeta \xrightarrow{1150} \beta+\zeta \xrightarrow{1025} \beta+\delta+\zeta \xrightarrow{850} \alpha+\beta+\gamma'$	β
Phase C	(Cr,αFe)$\xrightarrow{750}$ (Cr,αFe)+$\alpha_2+\eta$	$\beta \xrightarrow{1150} \alpha+\beta \xrightarrow{850} \gamma'$	β
	α_2 = FeAl η = $(Cr_{1-x}Fe_x)_2Al$ ζ_2 = Cr_5Al_8	α = (Cr) β = NiAl γ = Ni γ' = Ni_3Al ζ = Cr_5Al_8 δ = Ni_2Al_3	β = $(Fe_xNi_{1-x})Al_y$ γ = (Fe,Ni)

the laser treatment. From our analysis we can not conclude if all phases are present nor if one of them predominates, but the existance of Ni-Al and Fe-Al intermetallic compounds can lead to an improvement of the oxidation resistance of the material [24, 25, 26]. Phase B reaches the highest Al-content, and, as a consequence, Cr-Al compounds may start also to form together with the rest of the phases observed in phase C. Although the addition of Cr to Fe-Al compounds seems to be the most probable way to incorporate Cr as intermetallic compound (in the form of $(Cr_{1-x}Fe_x)_2Al$), other phases, like Cr_5Al_8 may also be present.

3 Conclusions

Laser surface alloying of Incoloy 800H with Al has been carried out, and the obtained material characterized by optical and electronic microscopy, and by XMA. Alloyed zones show a good aspect, homogeneity, and low rugosity. The effects of preparation parameters on the morphology of the modified surface have been evaluated. Three phases with different Al-content could be distinguished. The main phase consists of a solid solution with some Ni-Al intermetallic compounds inside. The other two phases, in form of precipitates, correspond mainly to Fe-Al and Fe-Cr-Al phases, respectively. The observed surface Al-enrichment, the considerable grain refining with respect to the base alloy, and the abundance of Ni-Al and Fe-Al intermetallic compounds, make this coating very interesting for high-temperature applications.

Acknowledgements. The authors wish to thank M. Larraz and P. Adeva for fruitful discussions. They also thank B. J. Fernández for his assistance in the rugosity measurements, and V. López for his help during the metallographic characterization.

References

1. W. J. Molloy, Adv. Mater. Process. **10/90**, 23 (1990).
2. T. Khan, Adv. Mater. Process. **1/90**, 19 (1990).
3. M. Yoshimura and F. H. Stott, MRS Bull. 20 (October 1994).
4. G. W. Goward, Mater. Sci. Technol. **2**, 194 (1986).
5. R. W. Richards, R. D. Jones, P. D. Clements, and H. Clarke, Int. Mater. Rev. **39**, 191 (1994).
6. G. C. Wood and F. H. Stott, Mater. Sci. Technol. **3**, 519 (1987).
7. J. Mazumder and J. Singh, in *Laser surface treatment of metals*, Vol. 115 of *NATO ASI Series E*, edited by C. W. Draper and P. Mazzoldi (Kluwer Academic Publishers, Dordrecht, Boston, London, 1986), p. 297.
8. J. J. de Damborenea and A. J. Vázquez, J. Mater. Sci. **27**, 1271 (1992).
9. B. C. Oberländer and E. Lugscheider, Mater. Sci. Technol. **8**, 657 (1992).
10. E. McCafferty and P. G. Moore, in *Laser Surface Treatment of Metals*, Vol. 115 of *NATO ASI Series E*, edited by C. W. Draper and P. Mazzoldi (Kluwer Academic Publishers, Dordrecht, Boston, London, 1986), p. 263.
11. J. J. de Damborenea and A. J. Vázquez, J. Mater. Sci. **28**, 4775 (1993).
12. J. de Damborenea, V. López, and A. J. Vázquez, Surf. Coat. Technol. **70**, 107 (1994).
13. J. H. Abboud, D. R. F. West, and R. D. Rawlings, Mater. Sci. Technol. **10**, 848 (1994). 2
14. W. Maocai and W. Weitao, Surf. Coat. Technol. **72**, 181 (1992).
15. J. H. Abboud and D. R. F. West, Mater. Sci. Technol. **7**, 353 (1991).
16. W. W. Steen, in *Laser surface treatment of metals*, Vol. 115 of *NATO ASI Series E*, edited by C. W. Draper and P. Mazzoldi (Kluwer Academic Publishers, Dordrecht, Boston, London, 1986), p. 369.
17. B. Grünenwald, E. Bischoff, J. Shen, and F. Dausinger, Mater. Sci. Eng. **8**, 637 (1992).
18. S. Zhu, F. Wang, H. Low, and W. Wu, Surf. Coat. Technol. **71**, 9 (1995).
19. F. Kostrubiec, J. Mater. Sci. **26**, 6044 (1991).
20. H. J. Hegge and J. T. M. de Hosson, J. Mater. Sci. **26**, 711 (1991).
21. C. Chan, J. Mazumder, and M. M. Chen, Metall. Trans. A **15A**, 2175 (1984).
22. S. Kou and Y. H. Wang, Metall. Trans. A **17A**, 2265 (1986).
23. *Ternary Alloys*, edited by G. Petzow and G. Effenberg (VCH, Weinheim, Germany, 1991), Vol. 3, p. 369; *ibid* p. 400; *ibid* Vol. 4, p. 309.
24. J. L. González-Carrasco, P. Adeva, and M. Aballe, Mater. Sci. Eng. A **128**, 231 (1990).
25. W. F. Gale, T. C. Totemeier, and J. E. King, Metall. Mater. Trans. A **26**, 949 (1995).
26. C. G. McKamey, J. H. DeVan, P. F. Tortorelly, and V. K. Sikka, J. Mater. Res. **6**, 1779 (1991).